Journal Name

ARTICLE TYPE

Cite this: DOI: 10.1039/xxxxxxxxxx

Polymer Assisted Deposition of epitaxial oxide thin films

José Manuel Vila-Fungueiriño,[a], Beatriz Rivas-Murias,[b] Juan Rubio-Zuazo,[c,d] Adrian Carretero-Genevrier,[a], Massimo Lazzari,[b] and Francisco Rivadulla[b*]

Received Date
Accepted Date

DOI: 10.1039/xxxxxxxxxx

www.rsc.org/journalname

Chemical solution methods for thin-film deposition constitute an affordable alternative to high-vacuum physical technologies, like Sputtering, Pulsed Laser Deposition (PLD) or Molecular Beam Epitaxy (MBE). Particularly, chemical methods have proven to be very suitable for producing functional films over large areas, especially in the relatively thick range, from >100 nm to microns. Also, their versatility to synthesize different types of materials, i.e. carbides, silicides, pnictides, oxides or chalcogenides, make them very attractive for a wide range of applications and studies. However, problems with surface/interface roughness, control of stoichiometry in multicationic or precisely-doped materials, and a lack of accurate control of the thickness in the thin limit range (< 20 nm) has weighed the competitiveness of these processes against high vacuum physical methods. This is particularly true in the case of multicationic oxide thin-films, which have experienced a frantic research activity in recent years associated with phenomena of interaction across atomically sharp interfaces; the vast majority of oxide thin films used in these studies were deposited under high vacuum. Here we review the Polymer Assisted Deposition (PAD) of epitaxial thin-films, with particular emphasis in the case of oxides. As we will show in this review, PAD is very versatile to produce different structural phases (perovskites, spinels, garnets, etc), demonstrating its competitiveness to produce oxide thin-films with the quality required for fundamental studies and applications, as well as its complementarity to physical methods for stabilizing metastable materials and composite heterostructures. We also provide a detailed step by step description of the most relevant chemical aspects of the method, in order to make it reproducible and attractive to laboratories with little experience in complex chemistry tasks.

1 Introduction

The development of experimental methods for atomic-scale growth of thin films with accurate control of thickness, stoichiometry and interface roughness was crucial for the advancement of materials science and technology.[1,2] Without any doubt, Molecular Beam Epitaxy (MBE)[3,4], Sputtering[5] and Pulsed Laser Deposition (PLD)[6] are among the most relevant. However, the cost of high-vacuum techniques prevents many research groups from having samples with the quality required for fundamental studies and applications. Another difficulty that must be overcomed is the issue of scalability, especially in PLD and MBE. Therefore, although high-vacuum methods offer unquestioned advantages like high crystal quality, precise control of composition and thickness at atomic-scale even for several unit cells thick films, more affordable alternatives are desirable. In this regard, chemical methods of deposition from a starting solution (Chemical Solution Deposition, CSD) are very appropriate for large area coatings and roll-to-roll manufacturing, with an easier implementation than high-vacuum methods.[7–9] The synthesis of inorganic thin films from a chemical solution encompasses a number of methods wich share a number of common steps: i) stabilization of the cations in the precursor solution; ii) homogeneous deposition on a substrate, normally by spin or dip coating; iii) thermal annealing in the adequate atmosphere to achieve the complete evaporation of the solvent and the crystallization of the film. Each of these steps poses several challenges, like the avoidance of undesired cross-reactions in the precursor solution, the achievement of a good adhesion to the substrate, or the homogeneous crystallization

[b] Institut dÉlectronique et des Systémes (IES) UMR 5214, CNRS. Université de Montpellier, 860 rue Saint Priest, 34095 Montpellier, France.
[b] Centro de Investigación en Química Biolóxica e Materiais Moleculares (CIQUS), Universidade de Santiago de Compostela, 15782-Santiago de Compostela, Spain; E-mail: f.rivadulla@usc.es
[c] Instituto de Ciencia de Materiales de Madrid (ICMM), Consejo Superior de Investigaciones Científicas (CSIC), C/Sor Juana Inés de la Cruz 3, 28049, Madrid, Spain.
[d] SpLine Spanish CRG Beamline at the ESRF, Grenoble, France.
† Electronic Supplementary Information (ESI) available: [details of any supplementary information available should be included here]. See DOI: 10.1039/b000000x/

of the final film, free of cracks and imperfections over large areas.[10–14] Diferent versions of CSD include, among others, the sol-gel[15–17], metal-organic decomposition (MOD)[18], or the chemical bath deposition (CBD)[19]. These were applied to the fabrication of a large variety of materials during the last decades, including ferromagnets[20,21], ferroelectrics[22,23], superconductors[24,25], transparent conductors[26,27], and energy storage materials[28,29]. However, producing continuous, single-crystal epitaxial thin films of functional oxides in the range below ≈20 nm has proven a goal very difficult to achieve. This is mainly due to the difficulties in controlling the thickness and surface roughness. Therefore, except in very specific cases,[30] the vast majority of studies in thin-films produced by chemical methods are constrained to polycrystalline materials, in the rage of thicknesses beyond 100 nm. These problems also hampered the production of complex multi-layered structures, constituting a serious drawback of CSD with respect to high-vacuum physical deposition methods, regarding for example the study of emergent phenomena in sharp interfaces.[31–33]

In this regard, the report by Jia *et al.*[34] of the growth of epitaxial $SrTiO_3$ (STO) thin films on $LaAlO_3$ (LAO) with very good crystalline and epitaxial quality by a water-based CSD method, was very important. Their strategy relied on the use of a water soluble polymer with functional -NH_2 groups that coordinate the cations, and prevent their hydrolysis. Moreover, the polymer provides the required viscosity for an adequate adhesion to the substrate during spin or dip-coating. Since this work, a large variety of thin-films and multilayers with different compositions (oxides, nitrides, carbides, etc.[35–37], see Figure1) and crystalline structures have been synthesized by this so-called polymer assisted deposition (PAD) method.[38–43]

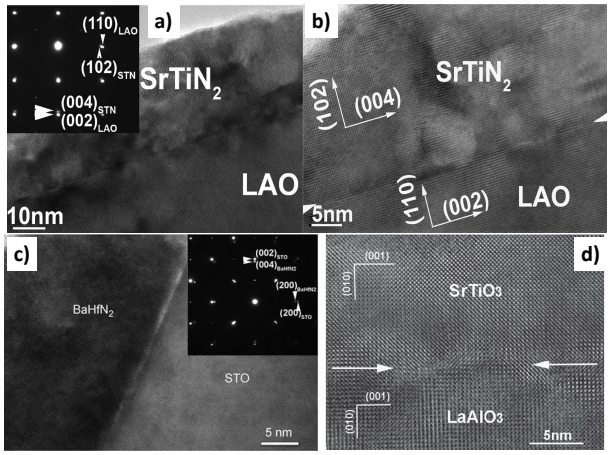

Fig. 1 Hig-resolution TEM pictures of different films prepared by PAD. $SrTiN_2$ and $BaHfN_2$ nitrides deposited on $LaAlO_3$ (a,b,c) and $SrTiO_3$ (d) depostied on $LaAlO_3$. Taken from references[34–36].

It is very important to emphasize at this point that PAD is a water-based method, where no complex chemical manipulation of toxic reactants or air/moisture sensitive precursors are involved.

Since the original publication of PAD, other CSD routes have also provided promising results for deposition of epitaxial oxide thin-films. Especially encouraging are those that involve aqueous precursors (green chemistry methods).[44] However, to prevent the formation of precipitates through hydrolysis or condensation is still challenging in aqueous-CSD. Also, counter ions and ligands from the precursors must be properly selected to be easily removed during thermal treatment.

Another interesting research direction is devoted to reducing energy consumption through low-temperature processing, aimed to produce crystalline films below 600°C.[45] This strategy can be applied to integrated functional oxides in flexible substrates. In this regard, Photochemical Solution Deposition promotes crystallization by the action of light in photosensitive precursors, lowering their crystallization temperature to temperatures as low as 325°C.[46]

The goal of this review is to provide an update of the most important results obtained by PAD in the synthesis of high quality thin-films, as well as of the challenges that remain to be solved. We restricted the discussion mostly to the case of oxides. We also provide a very detailed description of the relevant chemical parameters of PAD, in order to make it reproducible.

2 Preparation of stable solutions for Polymer Assisted Deposition of thin-films

PAD shares the three common steps to any CSD method, but it presents some key differences in the preparation of the precursor solution (see Figure 2).

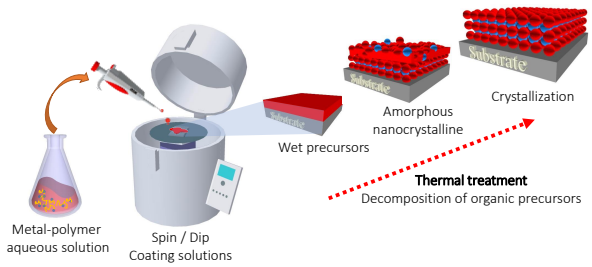

Fig. 2 Scheme of the different steps involved during the deposition of a thin-film from a precursor solution, CSD.

Most CSD methods rely on a starting solution in which the precursors are in a highly reactive state to undergo a chemical reaction; e.g.: hydrolysis, condensation, etc.[47] Reactive metal salts or metallorganic compounds such as alkoxides, are therefore manipulated (usually in organic solvents) to achieve this goal. But the high reactivity of the precursor solution poses the difficulty of controlling its stability with time, to prevent undesired side reactions. In other cases, the ligands and solvents just provide the correct viscosity of the solution to be deposited on the substrate: carboxylates (acetates, propionates, citrates, etc.), amines or β-diketonates are used as the metal source, and as the chelating agents.[48,49] The use of organic solvents of low molecular weight,[50–52] such as urea, alcohols (like ethylene glycol), xylene, acetylacetone or carboxylic acids (note that metal-hydrolysis restricts the use of water) results in partial evaporation with time, and poor stability of the metal solution which gives rise to phase segregation of the inorganic films.[53,54] High molecular weight

polymers, such as polyacrylic acid (PAA), polyvinyl alcohol (PVA), polyvinylpyrrolidone (PVP), polyvinyl butyral (PVB), polyethylene glycol (PEG) were also used to stabilize,[55] adjust the viscosity of the solution,[56,57] and reduce the formation of cracks in the film.[58] In this case the challenge is to achieve constant rheological properties of the solution and to avoid reactions of chelation, esterification, or polymerization which may occur in the media.

Opposite to these, one of the characteristics of PAD is the seek for a stable state of the cations in the precursor aqueous solution.[59] In order to do so, they are firmly coordinated to a polymer, which also controls the viscosity of the solution. Another factor that makes an important difference in PAD is that a separated precursor solution is prepared for each individual cation; mixing of different solutions in stoichiometric proportions is done just before the deposition of the multicationic film.

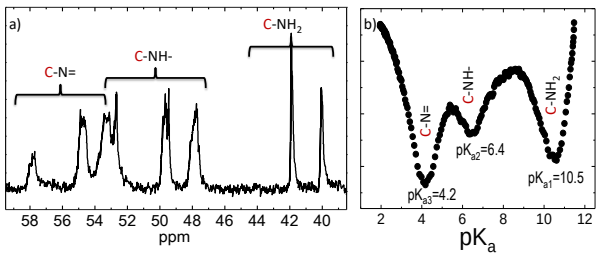

Fig. 3 a) ^{13}C-NMR of a sample of PEI, along with the asignment of the peaks to the carbon groups neighboring the primary (-NH_2), secondary (-NH-), and tertiary (-N=) amino groups, respectively. b) Acid/base titration of PEI in water, and the corresponding pK_a's of the different amino groups of the molecule. Taken from reference[43].

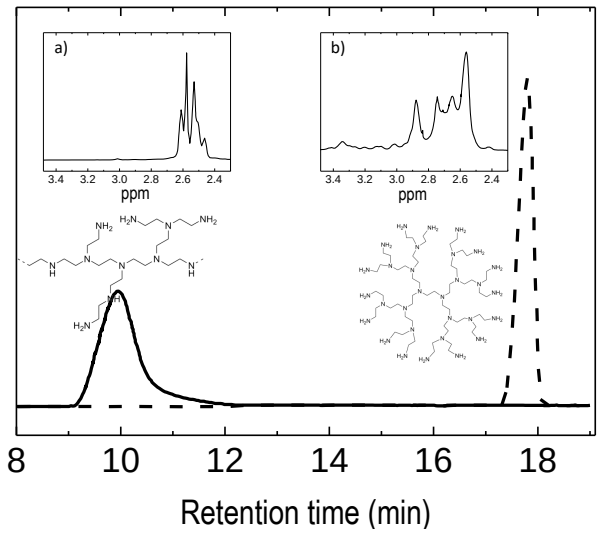

Fig. 4 Size exclusion chromatography of PEI. Two different species, with very different retention times are observed. They were identified by ^{1}H-NMR and assigned to a hyperbranched species of low molecular weight (1 kDa, inset b), and a more linear molecule of high molecular weight (193 kDa, inset a). Taken from reference[43].

The most widely used polymer in PAD is polyethyleneimine (PEI), although other polymers like PAA, or chitosan are also adequate.[60] PEI is a commercially available polymer, with high

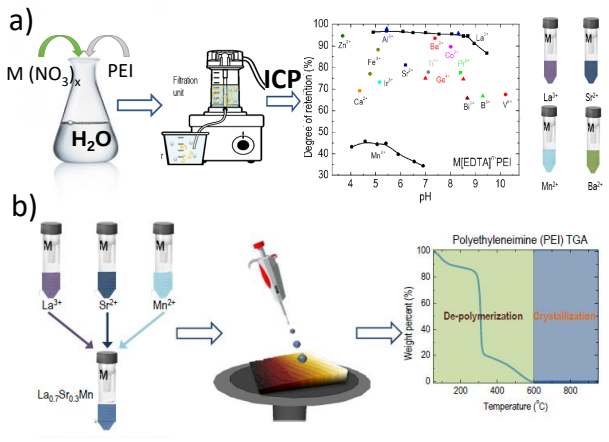

Fig. 5 Summary of the steps followed in PAD of a thin-film, from the preparation of the precursor solution, purification and ICP analysis of the cation content (shown in a), to the spin coating of the mixture and subsequent decomposition of the polymer and crystalization of the inorganic film by thermal annealing (shown in b)

molecular weight and good solubility in water. The branched structure of this molecule is characterized by the ratio of primary (-NH_2), secondary (-NH-), and tertiary (-N=) amino groups. The ratio -NH_2:-NH-:-N= can be measured experimentally by ^{13}C-NMR (see Figure 3a), and varies typically between 39:37:24 and 32:30:39 for most of the samples analyzed from different suppliers.[43] These functional groups can bind directly to a large number of ions in water solution,[61,62], and for optimum results -NH-:-N= should be kept between ≈1.1-1.5. On the other hand, although water solutions of PEI present a very high pH, -NH_2 and -NH- protonate below pH≈10 and pH≈6, respectively (see Figure 3b).[43] This is very important because only the non-protonated form of the PEI can form complexes with metal ions. Many transition metals and alkaline-earth metal-ions give rise to acidic water solutions, and hydrolize at pH even smaller than 7 in many cases. This problem can be solved by protecting the metal-ions with a chelating agent, normally ethylenediaminetetraacetic acid (EDTA), but also diethylenetriaminepentaacetic dianhydride, diethylenetriaminepentaacetic acid, etc. They form negatively charged complexes $[M(EDTA)^{n+}]^{(4-n)-}$ that can bind directly to protonated -NH_3^+ and -NH_2^+-. Chelation also provides an extra stabilization against metal hydrolysis, and allows a larger range of working pH.

A good starting point is to use 1 g of PEI and 1g of EDTA in 10 ml of water. This produces solutions with a viscosity η≈3-4 mPa s (η(H_2O at 20°C)=1.002 mPa s), optimum for spin coating deposition. Finally, the cationic salt is added to give a 1:1 molar ratio to EDTA. The order of the mixture must be properly considered, to avoid the hydrolysis of the metal.

On the other hand, a fundamental step during PAD is the purification of the precursor solution prior to deposition. This process is expected to remove non-coordinated species and undesired anions from the solution.[63]. However, it has been found that it has a more important role, removing also low-molecular weight portions of the polymer with very low solubility. An example of size exclusion chromatography of a commercial PEI is

shown in Figure 4. Apart from the main component at 180-200 kDalton, the chromatography shows another component of low molecular weight of 1-5 kDalton, with a hyperbranched structure with almost no -NH- groups, as found by ^{13}C- and ^{1}H-NMR.[43,64] Its molecular weight was also confirmed by pulse-field gradient NMR measurements, relating the attenuation of the signal during diffusion ordered spectroscopy (DOSY) with the diffusion coefficient.[43] These dendrimer-like molecules are insoluble in water and must be removed from the solution. For that reason, each solution is filtered and washed three times using 10 kDalton cutoff membranes in Amicon® Stirred Cells. Non-coordinated metal-ions or $[M(EDTA)^{n+}]^{(4-n)-}$, as well as counter cations, are also removed at this step, improving the purity of the solution. The permeated portions have values of η=1.01-1.08 mPa s, close to water. After this process, each solution is carefully analyzed by inductively coupled plasma optical emission spectrometry (ICP-OES) to determine the exact concentration of cations in the solution, and the degree of retention by the polymer (see Figure 5). Properly purified solutions of different cations are stable and most of them can be stored for months and even years.

Once the individual solutions are purified and analyzed they can be deposited on a substrate, typically by spin or dip-coating. For growing multicationic materials, the precursor solutions are mixed in the appropriate stoichiometric proportions, taking care of the final pH. The scheme of the whole process is summarized in Figure 5.

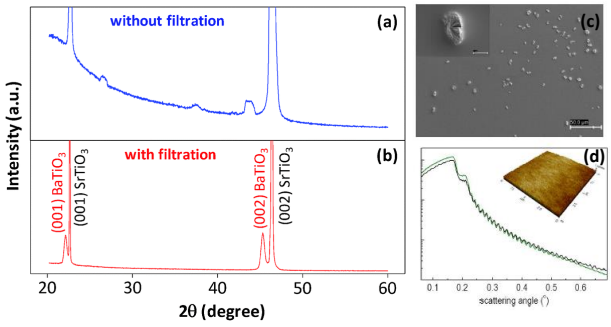

Fig. 6 a) and b) show the effect of filtration on the crystal structure of $BaTiO_3$ thin-films. Taken from Ref.[63]. c) SEM picture of a polymer film deposited on a Si substrate without filtration. An AFM picture of a polymer film deposited under similar conditions after filtration is shown in the inset of d). The reflectivity shows a thickess of ≈250 nm. taken from Ref.[43]

The importance of purification of the starting solution is shown in Figure 6. This is a limiting step in the production of high-quality thin-films over large areas, free of cracks and imperfections.

The final step is to anneal the polymeric film at high temperature, in an adequate atmosphere, to decompose the polymer and to crystallize the inorganic thin film. Thermogravimetric Analysis (TGA) indicated the complete degradation of the polymer above ≈550°C (see Figure 5b). The thermal stability of PEI prevents the formation of the film below this temperature (Figure 7).

An important aspect of PEI is that this polymer does not undergo a combustion, but rather an oxidant decomposition

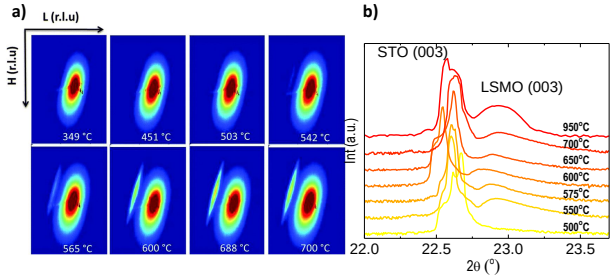

Fig. 7 Crystallization of the films after thermal annealing. The images in a) correspond to a series of x-ray reciprocal space maps of $BaTiO_3$ thin-films on STO (from Ref.[63]). In b) the x-ray patterns are shown for LSMO on STO. In both cases crystallization of the oxide occurs around the decomposition temperature the polymer, ≈550 °C, irrespective of the composition of the film.

to $NH_2CH{=}CH_2$, favoring less carbon contamination in the films.[63,65] This can be followed by IR-spectroscopy, observing the band of carbonyl bond formation ca 1700 cm^{-1}, overlapped to amine bending at 1642 cm^{-1}, above at 300°C.[66] Annealing above 600°C produces a complete decomposition of the polymer in volatile species, without any remain of organic material in the sample. EDTA also decomposes to acetic acid, formic acid, and ethylenediamine.[67] Furthermore, the slow decomposition of the polymer, at a final temperature close to the crystallization temperature of the inorganic film from an amorphous precursor, promotes the formation of the inorganic film at a very slow rate, close to thermodynamic equilibrium conditions, and promotes high crystallinity and quality.

By following this simple procedure many different compounds have been grown: single[68–81] and multicationic oxides[38–40,60,82–92], nitrides[35,36,93–97], carbides[98–100] and pure element semiconductors, like Germanium[101]. Multicationic oxides are probably the more interesting category due to their large variety of compositions, crystal structures and functionalities. For this, from now on we will refer only to the results on epitaxial thin-film oxide synthesized by PAD.

3 PAD deposition of epitaxial oxide thin-films

3.1 Control of stoichiometry and thickness over large areas

Epitaxial growth of a film on a substrate refers to the case in which a structural coherence is maintained between both crystalline structures.[102] This implies not only an oriented relationship to the substrate, but also a total structural coherence defined by the crystallographic lattice matching to the substrate, opening an avenue to tailor their physical properties by epitaxial strain engineering.[103,104]

Mixed-valence Mn-oxoperovskites of general formula $Ln^{3+}_{1-x}A^{2+}_{x}MnO_3$ (Ln=lanthanide, A=alkaline-earth) constitute a family of materials particularly suitable to test the control achieved by PAD over the stoichiometric and thickness over large areas, due to the extreme sensitivity of their magnetic and transport properties to small variations of composition.[105]

Some results showing the stoichiometry and thickness con-

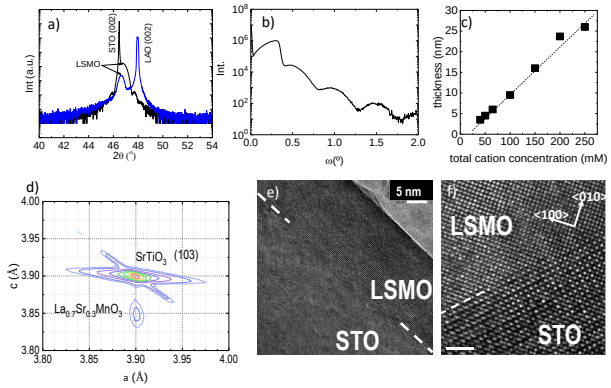

Fig. 8 a) X-ray diffraction of a thin-film of LSMO deposited on LAO and STO. b) X-ray reflectivity of one of these films, showing the charateristic Kiessig fringes of a low interface/surface roughness. c) Total film thickness vs. cation concentration in the solution. d) x-ray map of LSMO on STO, around the (-103) reflection. The image demonstrates the good epitaxial matching between the film and the substrate. e) High-resolution TEM image of a cross-section lamella of LSMO on STO. f) Magnification of the interface in e).

trol in the films are shown in Figures 8 and 9 for thin films of $La_{0.7}Sr_{0.3}MnO_3$ (LSMO) and $La_{1-x}Ca_xMnO_3$ on STO, respectively. There is a good correspondence between the nominal and the actual ratio of La/Ca in the films. The behavior in terms of temperature dependence of the electrical resistivity and magnetization of the PAD samples compared very well with the samples prepared by PLD.[106] These results demonstrate the accurate control over the stoichiometry in multicationic compounds that can be achieved by PAD.

Moreover, X-ray diffraction, reflectivity and cross-section TEM analysis demonstrate the low surface/interface roughness, and epitaxy of the layers. Also, as shown in Figure 8c), an excellent control over the thickness (from ≈3.5-30 nm) can be achieved through the total concentration of cations in the precursor solution. Multiple depositions result in thicker films without loosing crystalline quality.

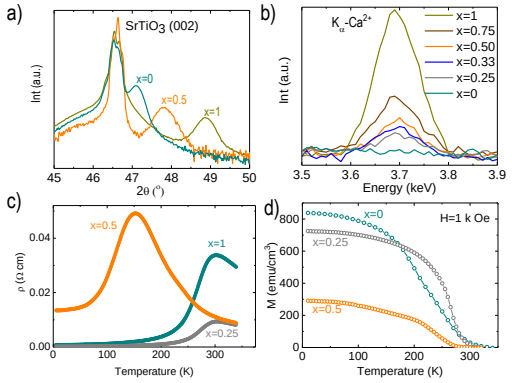

Fig. 9 a) X-ray diffraction and b) detail of the Ca element EDX analysis at 3.69 KeV for $La_{1-x}Ca_xMnO_3$ films. The temperature dependence of the electrical resistivity and magnetization, are shown for different values of the La/Ca ratio in c) and d), respectively.

Finally, the quality of the layers deposited by PAD is maintained over relatively large substrates of 1" (see Figure 10).

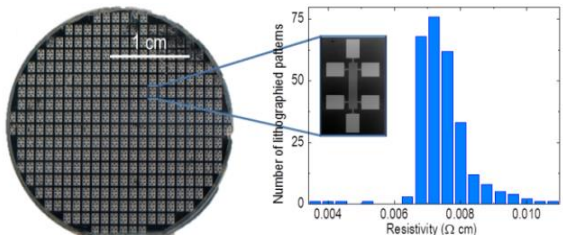

Fig. 10 1'-STO substrate with a 18 nm thick LSMO thin-film deposited by PAD. Optical lithography and lift-off was used to define 324 Hall-bars (inset picture) and the electrical resistivity was measured in all of them. The distribution of the values at room temperature are shown in the hystogram.[43]

Therefore, PAD is very suitable for coating large areas with very thin epitaxial films, keeping the quality of the films to accomplish the requirements to produce devices.

3.2 Synthesis of epitaxial multilayers

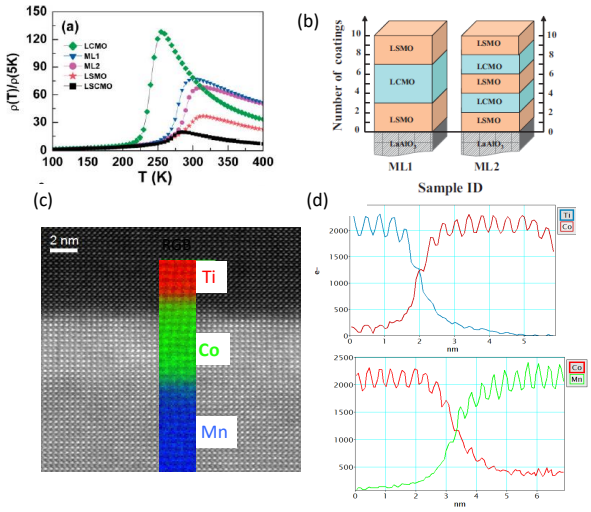

Fig. 11 a,b) Schematic diagram of the multilayer-coated LSMO/LCMO films and the corresponding normalized resistivity, from reference[107]. c,d) High-resolution of electron microscopy images and EELS analysis of $LaCoO_3$(3.5 nm)/LSMO(22 nm) deposited by PAD in STO, from references[108,109].

The precise control of the interface roughness in a multilayer heterostructure needed to fabricate a tunnel junctions, is normally beyond the capabilities of CSD methods. For that reason, chemical methods are not usually appropriated for the study of subtle phenomena at interfaces of epitaxial systems. However, the precise control over the stoichiometry and roughness achieved by PAD makes this method suitable for the fabrication of epitaxial heterostructures. Jain et al.[107] prepared multilayers of $La_{0.67}Sr_{0.33}MnO_3/La_{0.67}Ca_{0.33}MnO_3$, with an excellent control over their magnetoresistive response at room temperature. Vila-Fungueiriño et al.[108,109] fabricated tunnel junctions of $LaCoO_3$(3.5 nm)/$La_{0.67}Sr_{0.33}MnO_3$ (Figure 11. The tunnelling conduction was verified by Conductive Atomic Force Microscopy

(C-AFM). From the fitting of current-voltage curves to the Simmons model were obtained two parameters: (1) the thickness of the barrier, t=3.2 nm, which was very similar to that obtained by TEM (3.5 nm) and (2) the height of the barrier, E=0.4 eV.[108] The latter value was very close to the obtained in barriers of STO deposited by PLD[110], demonstrating that ultra-thin layers of LCO prepared by PAD retained a good insulator character and can be used as tunneling barriers in combination with LSMO at room temperature.

3.3 Thermodynamic stabilization of complex oxides

Some materials are difficult to grow as thin films, particularly using PLD and other methods in which growth is a non-equilibrium process. This is the case of many materials with complex structures or chemical composition.

There are also situations in which the characteristic growth conditions of PAD can be advantageous for the stabilization of a particular phase of a given material. For example, epitaxial stress in thin-film oxo-perovskites is accomodated through a complex rotation of the MO_6 octahedra[106]. This is different depending on the degree of strain and the symmetry of the substrate,[111] therefore affecting the properties of the film. For the case of LSMO, it has been shown that the rotation different pattern is stabilized in thin-films grown by PLD (Cmcm) and PAD (I4/mmm).[106] This is an important result, because it demonstrates that the nature and magnitude of the magnetic anisotropy in LSMO (and other materials) can be tuned by the thermodynamic parameters during thin-film deposition.

Figure 12 shows X-ray synchrotron reciprocal space maps around different reflections of two films of LSMO on STO with different thicknesses. The in-plane domain size is as large as 78 nm and 205 nm for films of 5 nm and 20 nm thick, respectively, showing the excellent crystalline quality of the films.

From the fittings of the integrated intensities of different reflections, the interface of both films was determined to be pure TiO_2-$La_{0.7}Sr_{0.3}O$, in all cases. These results reflect the impact of the slow growth conditions of PAD, close to thermodynamic equilibrium conditions, on the final properties of the material.

PAD can be useful to synthesize complex phases which imply complex cationic ordering which suggest thermodynamic growth conditions to be more adequate.

An interesting example are thermoelectric misfit cobalt oxides.[112,113] Deposition of thin films by PLD or Sputtering is really complicated as the stoichiometric transfer from the target normally produces amorphous areas[114] close to the interface to the substrate. This is an important drawback for the stacking of these materials in a multilayer heterostructure. However, c-axis oriented single phase of nominal composition of $Ca_3Co_4O_9$, $Sr_3Co_4O_9$ and $[Bi_{1.74}Sr_2O_4][CoO_2]_{1.82}$, $[Bi_2Ba_{1.8}Co_{0.2}O_4][CoO_2]_2$, and $[Bi_{1.68}Ca_2O_4][CoO_2]_{1.69}$) rock salt layers were successfully deposited on LAO by PAD (13 a), b).[115] The growth of the ordered structure from the substrate interface is due to the bottom-up slow crystallization of an epitaxial rock-salt layer on top of the LAO substrate, with a relationship (001) BiORS||(001)LAO; [110]BiORS ||[100]LAO.

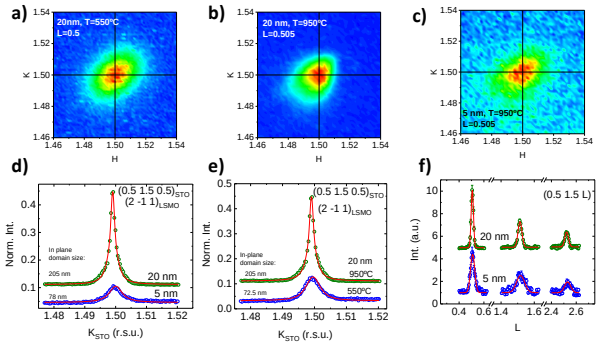

Fig. 12 X-ray synchrotron reciprocal space maps (RSM) around different reflections of different films of LSMO on STO. a) and b) show the comparison of two identical films of 20 nm, crystallized at 550^{0}C and 950^{0}C, respectively. The structure of a 5 nm film prepared at 950^{0}C is shown in c). The cristalline quality of the layers is very good already after decomposition of the polymer at around 550^{0}C. In the lower panels we show the fittings of different reflections of the films, in order to extract the structural parameters (see text).

$Y_3Fe_5O_{12}$ (YIG) is another example of a material with a complex structure, in which Fe^{3+} ions occupy different octahedral:tetrahedral sites, in a precise 2:3 distribution which determines its final properties. The synthesis of epitaxial thin-films ($\approx$15 nm) of YIG was also recently reported by PAD.[116] The slow growth of the films in quasi-equilibrium conditions produce an excellent chemical, crystalline and magnetic homogeneity. As a result, a narrow ferromagnetic resonance (long spin relaxation time), has been reported in YIG grown by PAD. This is an important step forward for the use of chemical methods in the production of nanometer-thick YIG films with the quality required for spintronic devices and other high-frequency applications.

This thermodynamic growth regime characteristic of PAD can be further exploited to synthesize metastable phases of technologically relevant materials, difficult to achieve by other methods. One example is ZnO, a n-type semiconductor which can be doped to increase its electrical conductivity, while maintaining its transparency, chemical and thermal stability. Thin films of luminiscent ZnO were grown by PAD in 2005,[69] and latter in 2012 the effect of vacancies over their magnetic properties was studied.[51] These properties call for the development of affordable synthetic methods suitable for deposition over large areas. Actually, ZnO can be grown by PAD with either $(11\bar{2}0)$ or (0001) orientation controlling the substrate strain and thermal annealing atmosphere, demonstrating that PAD could be an affordable route to access the anisotropic properties of ZnO thin films (Figure 14).

Self-assembled epitaxial nanostructures have been prepared by PAD combining materials with different crystal structures (perovskites, spinels, etc). These include nanocomposite thin-films of ferroelectric $BaTiO_3$ embebed in ferrimagnetic $NiFe_2O_4$[117]; multiferroic structures of $BaTiO_3$ in $CoFe_2O_4$[118]; hard-magnet $CoFe_2O_4$ diluted in diamagnetic $SrTiO_3$ and MgO (15);[84] or $La_{0.67}Ca_{0.33}MnO_3$:NiO and $La_{0.67}Ca_{0.33}MnO_3$:Co_3O_4 nanocomposite films with enhanced low-field magnetoresistance.[119]

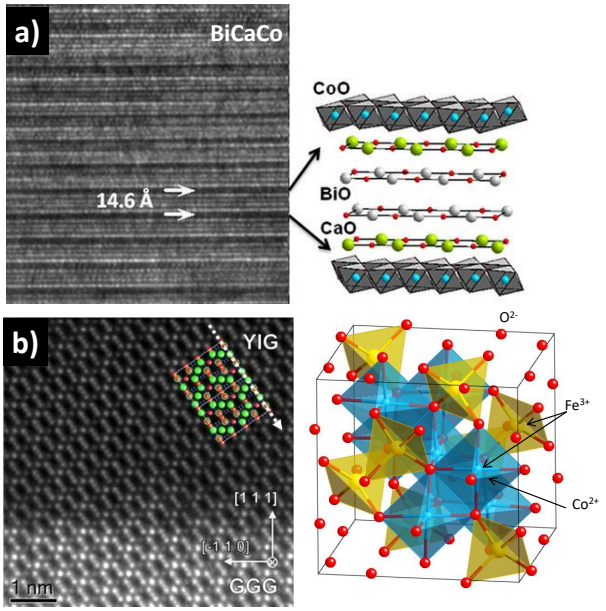

Fig. 13 a) TEM image (and schematic crystal structure) of misfit cobalt oxide $[Bi_{1.68}Ca_2O_4][CoO_2]_{1.69}$,[115] and b) YIG,[116] deposited by PAD.

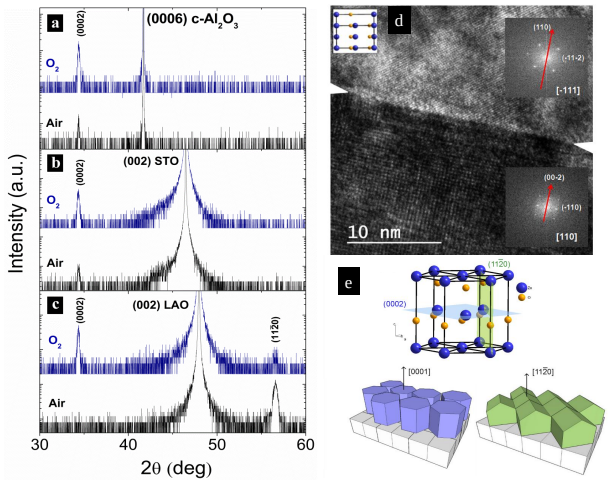

Fig. 14 2θ-ω XRD patterns for ZnO films grown on c-Al_2O_3 (a), STO (b) and LAO (c) substrates under oxygen and air atmosphere. The position of the (0002) and (11$\bar{2}$0) peaks of ZnO is indicated. d) TEM cross-section image of ZnO film deposited on LAO in air with Fourier transforms for the film and the substrate. Inset: Cell orientation in the film. e) (11$\bar{2}$0) and (0002) planes of ZnO wurzite crystal structure. Lattice arrangement of epitaxial ZnO grown on LAO with [0001] and [11$\bar{2}$0] orientations

3.4 Integration of functional oxides on Silicon

The capability of PAD to stabilize complex thin films difficult to produce by classical deposition methods, opens a new route to complement some physical deposition methods to integrate functional oxides on silicon. The combination of the different properties of crystalline oxides with semiconductor technology could improve the functionality and the performance of the existing materials in the fields of microelectronics, optoelectronics, and spintronics.

Deposition of epitaxial oxides on silicon is a complex task due to their compositional and structural dissimilarities, as well as to the thermodynamic instabiltiy of many oxides in contact with silicon.[120,121] Moreover, the almost unavoidalbe formation of a thin SiO_2 layer at the Si/oxide interface hinders the epitaxial stabilization.

Bakaul *et al.*[122] used an original approach, in which epitaxial thin films of ferroelectric oxides were first grown by PLD on a lattice-matched substrate with a thin sacrificial layer. Once released from the buffer, the film is transferred onto Si and other substrates. This procedure was sucessfully applied to the production of $Pb(Zr_{0.2}Ti_{0.8})O_3$, $(CaTiO_3/SrTiO_3)_6$ superlattices and $SrRuO_3/BiFeO_3/CoFeB/Pt$ multilayers. However, this method is tedious and not difficult to scale up.

To overcome these important obstacles, an buffer layer (normally an oxyde or a nitride)[125,126] is grown at high vacuum on top of bare Si, prior to deposition of a complex oxide. This opens the possibility of using chemical solution methods to further integrate complex oxides on these functionalized Si substrates. In this case, the versatility of PAD can be extended to create more complex structures than dense thin-films, which adds extra functionality to these materials. An example is shown in Figure 16.[123,124,127]

The combination of PAD with physical methods like MBE offers also some interesting possibilities. The deposition of textured bottom electrodes of LSMO for ferroelectric $BaTiO_3$ was demonstrated by A. Gómez *et al.*[124] Interestingly, apart from the characteristic ferroelectric properties of BTO, the authors also proved that the microstructure induced in the LSMO promotes a new property flexoelectric-like response in BTO. In these unique nanostructures produced by MBE/PAD combination, the ferroelectric domains can be reversed by a bias voltage and/or by a mechanical force. The change in the conductivity is not volatile, opening the possibility to fabricate memory-devices.

4 Conclusions and challenges

In this paper we have reviewed a series of recent developments of PAD for deposition of epitaxial thin-films of complex oxides, in the thickness range < 20 nm, where other chemical methods start to fail. The critical chemical aspects of PAD have been well characterized an optimized during the last years. As a result, the process is now mature enough to reach the level of control over the thickness, stoichiometry and roughness required to compete with physical deposition methods in many applications. The challenges and opportunities that offers PAD for the future are enormous. For example, it will be certainly interesting to study deeper the mechanism of thin-film growth, with in-situ monitoring the crystallization of the film at the first stages. Gaining control over this part of the processes will help stabilizing metastable phases, difficult to achieve by physical methods. Also, conformal coating of large and irregular areas,[75] as well the combination with other nanostructures such as nanoparticles to obtain composites with new properties, are still insufficiently explored.

Another important path that must be pursued is the seek for more effective complexation agents and polymers, specific to particular cations, to avoid the hydrolysis or undesired reactions in

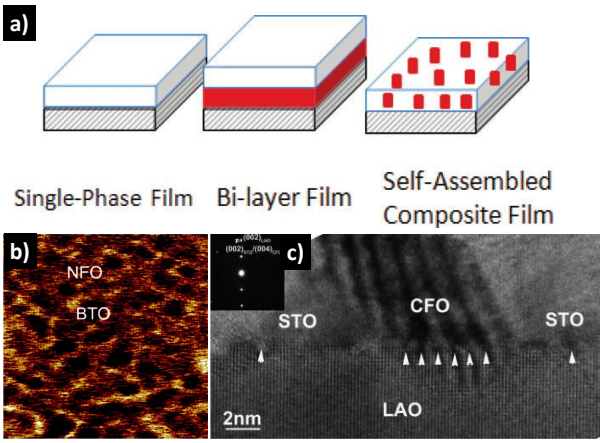

Fig. 15 a) Schematic structure of the epitaxial self-assembled nanocomposites prepared by PAD.[84] b) AFM of epitaxial nanocomposites of $BaTiO_3$-$NiFe_2O_4$,[117] and TEM of $CoFe_2O_4$:$SrTiO_3$, c), deposited by PAD.[84]

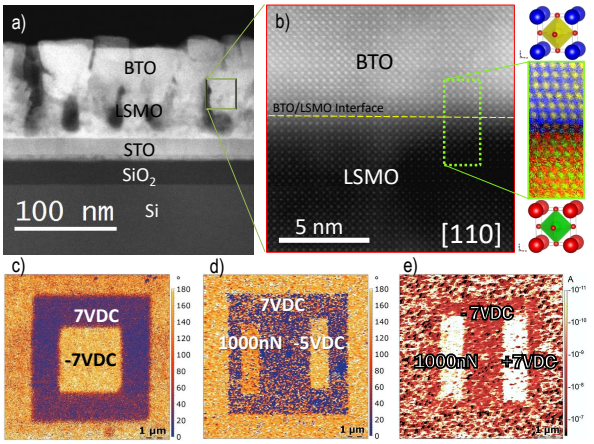

Fig. 16 a) Low magnification Z-contrast image of a porous epitaxial BTO/LSMO/STO/Si(001) multilayer viewed along the [110] Si axis. b) High resolution Z-contrast image of the BTO/LSMO interface viewed along the Si [110]-crystallographic direction, and higher resolution Z-contrast image of the coherent interface between the BTO and LSMO layers. Phase image of a 45 nm thick $BaTiO_3$ film after the generation of the downward-oriented ferroelectric domains by electrical poling (c), and mechanical loading force (d). e) Mapping of electrical current of the same film showing the piezo-driven resistance switching between two different resistance states by electrical poling and mechanical load. Taken from Refs.[123,124]

the precursor solution. This is important for the chemistry of 4*d* and 5*d* ions, like Iridium oxides, with important applications in catalysis,[128,129] as well as for the stabilization of single-valence ions, like Li^+, as a first step towards the synthesis of films of layered ionic conductors, with applications in batteries.[87]

Another interesting direction of research is the complementation of polymer assisted deposition with advanced crystallization methods, as an alternative to furnace-heating. For example, Breckenfeld *et al.*[130] used a pulsed-UV-laser to promote crystallization and particle growth in thin-films deposited below ≈450°C. They also showed the potential of laser-induced transfer from VO_2 films for printing applications. The possibility of using UV-light to promote decomposition of the polymer and crystallization of the inorganic film at lower temperatures also offers tremendous possibilities.[45]

These are crucial aspects for the integration of films in plastic substrates, where the temperature of the synthesis should be reduced down to ≈350°C, at least. A successful approach to this task will include the exploratory synthesis of new polymers, with lower decomposition temperatures, but maintaining optimal rheological and complexation properties. The use of alternative solvents to water is also another possibility, although the environmental aspects should be kept in mind in this case.

Therefore, the number of open research lines related to PAD is still enormous, like the number of possible applications. The succes of many of them will imply a collaborative effort of interdisciplinary research teams, with experience in polymer synthetic chemistry, inorganic and solid state chemistry, and materials science.

Acknowledgments. We acknowledge financial support by the Ministry of Science of Spain (Projects No. MAT2016-80762-R), the Consellería de Cultura, Educación e Ordenación Universitaria (ED431F 2016/008, and Centro singular de investigación de Galicia accreditation 2016-2019, ED431G/09), the European Regional Development Fund (ERDF). ACG and JMVF acknowledge the financial support from the French Agence Nationale pour la Recherche (ANR), project Q-NOSS ANR ANR-16-CE09-0006-01. We also acknowledge the Spanish Ministerio de Economia, Industria y Competitividad and Consejo Superior de Investigaciones Científicas for financial support and for provision of synchrotron radiation facilities at beamline BM25-SpLine at the European Synchrotron.

References

1 J. Anderson, *Thin Solid Films*, 1972, **12**, 1–15.
2 H. Frey, in *Handbook of Thin-Film Technology*, Springer Berlin Heidelberg, Berlin, Heidelberg, 2015, pp. 1–3.
3 A. Y. Cho and J. R. Arthur, *Progress in Solid State Chemistry*, 1975, **10**, 157–191.
4 M. Opel, *Journal of Physics D: Applied Physics*, 2012, **45**, year.
5 I. Safi, *Surface and Coatings Technology*, 2000, **127**, 203–219.
6 D. B. Chrisey and G. K. Hubler, *Pulsed laser deposition of thin films*, John Wiley and Sons, 1994.
7 D. S. Hecht and R. B. Kaner, *MRS Bulletin*, 2011, **36**, 749–755.
8 Z. Tan, L. Li, C. Cui, Y. Ding, Q. Xu, S. Li, D. Qian and Y. Li, *Journal of Physical Chemistry C*, 2012, **116**, 18626–18632.
9 W. Ke, G. Fang, Q. Liu, L. Xiong, P. Qin, H. Tao, J. Wang, H. Lei, B. Li, J. Wan, G. Yang and Y. Yan, *Journal of the American Chemical Society*, 2015, **137**, 6730–6733.
10 F. F. Lange, *Science*, 1996, **273**, 903–909.
11 R. W. Schwartz, *Chemistry of Materials*, 1997, **9**, 2325–2340.
12 R. W. Schwartz, T. Schneller and R. Waser, *Comptes Rendus Chimie*, 2004, **7**, 433–461.

13 D. B. Mitzi, *Solution Processing of Inorganic Materials*, John Wiley and Sons, 2008, pp. 1–497.

14 T. Schneller, R. Waser, M. Kosec and D. Payne, *Chemical solution deposition of functional oxide thin films*, Springer-Verlag Wien, 2013, pp. 1–796.

15 J. Livage, M. Henry and C. Sanchez, *Progress in Solid State Chemistry*, 1988, **18**, 259–341.

16 L. L. Hench and J. K. West, *Chemical Reviews*, 1990, **90**, 33–72.

17 C. J. Brinker and G. W. Scherer, *Sol-Gel Science: The Physics and Chemistry of Sol-Gel Processing*, Elsevier Inc., 2013, pp. 1–908.

18 J. Fukushima, K. Kodaira and T. Matsushita, *Journal of Materials Science*, 1984, **19**, 595–598.

19 R. S. Mane and C. D. Lokhande, *Materials Chemistry and Physics*, 2000, **65**, 1–31.

20 U. Hasenkox, C. Mitze and R. Waser, *Journal of the American Ceramic Society*, 1997, **80**, 2709–2713.

21 J. H. Park, M. G. Kim, H. M. Jang, S. Ryu and Y. M. Kim, *Applied Physics Letters*, 2004, **84**, 1338–1340.

22 M. Klee, R. Eusemann, R. Waser, W. Brand and H. Van Hal, *Journal of Applied Physics*, 1992, **72**, 1566–1576.

23 D. A. Barrow, T. E. Petroff, R. P. Tandon and M. Sayer, *Journal of Applied Physics*, 1997, **81**, 876–881.

24 M. E. Gross, M. Hong, S. H. Liou, P. K. Gallagher and J. Kwo, *Applied Physics Letters*, 1988, **52**, 160–162.

25 P. C. McIntyre, M. J. Cima and M. F. Ng, *Journal of Applied Physics*, 1990, **68**, 4183–4187.

26 J. H. Lee, K. H. Ko and B. O. Park, *Journal of Crystal Growth*, 2003, **247**, 119–125.

27 H. C. Cheng, C. F. Chen and C. Y. Tsay, *Applied Physics Letters*, 2007, **90**, year.

28 S. C. Pang, M. A. Anderson and T. W. Chapman, *Journal of the Electrochemical Society*, 2000, **147**, 444–450.

29 T. Brezesinski, J. Wang, J. Polleux, B. Dunn and S. H. Tolbert, *Journal of the American Chemical Society*, 2009, **131**, 1802–1809.

30 A. Ron, A. Hevroni, E. Maniv, M. Mograbi, L. Jin, C.-L. Jia, K. W. Urban, G. Markovich and Y. Dagan, *Advanced Materials Interfaces*, 2017, **4**, 1700688—-n/a.

31 J. Chakhalian, J. W. Freeland, G. Srajer, J. Strempfer, G. Khaliullin, J. C. Cezar, T. Charlton, R. Dalgliesh, C. Bernhard, G. Cristiani, H. U. Habermeier and B. Keimer, *Nature Physics*, 2006, **2**, 244–248.

32 H. U. Habermeier, *Materials Today*, **10**, 34–43.

33 H. Y. Hwang, Y. Iwasa, M. Kawasaki, B. Keimer, N. Nagaosa and Y. Tokura, *Nature Materials*, 2012, **11**, 103–113.

34 Q. X. Jia, T. M. McCleskey, A. K. Burrell, Y. Lin, G. E. Collis, H. Wang, A. D. Q. Li and S. R. Foltyn, *Nat Mater*, 2004, **3**, 529–532.

35 H. Luo, H. Wang, Z. Bi, G. Zou, T. McCleskey, A. Burrell, E. Bauer, M. Hawley, Y. Wang and Q. Jia, *Angewandte Chemie International Edition*, 2009, **48**, 1490–1493.

36 H. Luo, H. Wang, Z. Bi, D. M. Feldmann, Y. Wang, A. K. Burrell, T. M. McCleskey, E. Bauer, M. E. Hawley and Q. Jia, *Journal of the American Chemical Society*, 2008, **130**, 15224–15225.

37 G. F. Zou, J. Zhao, H. M. Luo, T. M. McCleskey, A. K. Burrell and Q. X. Jia, *Chem. Soc. Rev.*, 2013, **42**, 439–449.

38 Y. Lin, J. S. Lee, H. Wang, Y. Li, S. R. Foltyn, Q. X. Jia, G. E. Collis, A. K. Burrell and T. M. McCleskey, *Applied Physics Letters*, 2004, **85**, 5007–5009.

39 H. Luo, M. Jain, T. M. McCleskey, E. Bauer, A. K. Burrell and Q. Jia, *Advanced Materials*, 2007, **19**, 3604–3607.

40 H. Luo, A. H. Mueller, T. M. McCleskey, A. K. Burrell, E. Bauer and Q. X. Jia, *Journal of Physical Chemistry C*, 2008, **112**, 6099–6102.

41 L. Kang, Y. Gao, H. Luo, Z. Chen, J. Du and Z. Zhang, *ACS Applied Materials and Interfaces*, 2011, **3**, 135–138.

42 F. Rivadulla, Z. Bi, E. Bauer, B. Rivas-Murias, J. M. Vila-FungueiriÃśo and Q. Jia, *Chemistry of Materials*, 2013, **25**, 55–58.

43 J. M. Vila-FungueiriÃśo, B. Rivas-Murias, B. RodrÃ■guez-GonzÃąlez, O. Txoperena, D. Ciudad, L. E. Hueso, M. Lazzari and F. Rivadulla, *ACS Applied Materials & Interfaces*, 2015, **7**, 5410–5414.

44 M. K. Van Bael, A. Hardy and J. Mullens, in *Aqueous precursor systems*, 2013, vol. 9783211993118, pp. 93–140.

45 I. Bretos, R. JimÃľnez, J. Ricote and M. L. Calzada, *Chemical Society Reviews*, 2018, **47**, 291–308.

46 I. Bretos, R. JimÃľnez, D. PÃľrez-Mezcua, N. Salazar, J. Ricote and M. L. Calzada, *Advanced Materials*, 2015, **27**, 2608–2613.

47 D. C. Bradley, *Chemical Reviews*, 1989, **89**, 1317–1322.

48 U. Hasenkox, S. Hoffmann and R. Waser, *Journal of Sol-Gel Science and Technology*, 1998, **12**, 67–79.

49 U. Choppali and B. P. Gorman, *Journal of Luminescence*, **128**, 1641–1648.

50 A. Galembeck and O. L. Alves, *Thin Solid Films*, 2000, **365**, 90–93.

51 H. M. Zhou, D. Q. Yi, Z. M. Yu, L. R. Xiao and J. Li, *Thin Solid Films*, 2007, **515**, 6909–6914.

52 M. T. Soo, N. Prastomo, A. Matsuda, G. Kawamura, H. Muto, A. F. M. Noor, Z. Lockman and K. Y. Cheong, *Applied Surface Science*, 2012, **258**, 5250–5258.

53 A. H. Carim, B. A. Tuttle, D. H. Doughty and S. L. Martinez, *Journal of the American Ceramic Society*, 1991, **74**, 1455–1458.

54 C. C. Hsueh, *Journal of Materials Research*, 1991, **6**, 2208–2217.

55 C. Santato, M. Odziemkowski, M. Ulmann and J. Augustynski, *Journal of the American Chemical Society*, 2001, **123**, 10639–10649.

56 W. T. Wang, G. Li, M. H. Pu, R. P. Sun, H. M. Zhou, Y. Zhang, H. Zhang, Y. Yang, C. H. Cheng and Y. Zhao, *Physica C: Superconductivity and its Applications*, 2008, **468**, 1563–1566.

57 Y. R. Patta, D. E. Wesolowski and M. J. Cima, *Physica C: Superconductivity and its Applications*, 2009, **469**, 129–134.

58 H. Kozuka, M. Kajimura, T. Hirano and K. Katayama, *10th International Workshop pn Glass and Ceramics, Hybrids and Nanocomposites from Gels*, 2000, **19**, 205–209.

59 L. Fei, M. Naeemi, G. Zou and H. Luo, *The Chemical Record*, 2013, **13**, 85–101.

60 H. M. Luo, M. Jain, S. A. Baily, T. M. McCleskey, A. K. Burrell, E. Bauer, R. F. DePaula, P. C. Dowden, L. Civale and Q. X. Jia, *J Phys Chem B*, 2007, **111**, 7497–500.

61 T. Takagishi, S. Okuda, N. Kuroki and H. Kozuka, *Journal of Polymer Science: Polymer Chemistry Edition*, 1985, **23**, 2109–2116.

62 S. I. Kadioglu, L. Yilmaz and H. O. Ozbelge, *Separation Science and Technology*, 2009, **44**, 2559–2581.

63 T. M. McCleskey, P. Shi, E. Bauer, M. J. Highland, J. A. Eastman, Z. X. Bi, P. H. Fuoss, P. M. Baldo, W. Ren, B. L. Scott, A. K. Burrell and Q. X. Jia, *Chem Soc Rev*, 2014, **43**, 2141–6.

64 O. Yemul and T. Imae, *Colloid and Polymer Science*, 2008, **286**, 747–752.

65 A. K. Burrell, T. Mark McCleskey and Q. X. Jia, *Chemical Communications*, 2008, 1271–1277.

66 S. A. Idris, O. A. Mkhatresh and F. Heatley, *Polymer International*, 2006, **55**, 1040–1048.

67 I. E. Kirillina, V. N. Voronov, A. M. Dolgonosov and M. A. Lazeikina, *Thermal Engineering*, 1988, **35**, 538–539.

68 Y. Lin, H. Wang, M. E. Hawley, S. R. Foltyn, Q. X. Jia, G. E. Collis, A. K. Burrell and T. M. McCleskey, *Applied Physics Letters*, 2004, **85**, 3426–3428.

69 Y. Lin, J. Xie, H. Wang, Y. Li, C. Chavez, S. Lee, S. R. Foltyn, S. A. Crooker, A. K. Burrell, T. M. McCleskey and Q. X. Jia, *Thin Solid Films*, 2005, **492**, 101–104.

70 P. Shukla, E. M. Minogue, T. M. McCleskey, Q. X. Jia, Y. Lin, P. Lu and A. K. Burrell, *Chemical Communications*, 2006, 847–849.

71 A. K. Burrell, T. M. McCleskey, P. Shukla, H. Wang, T. Durakiewicz, D. P. Moore, C. G. Olson, J. J. Joyce and Q. Jia, *Advanced Materials*, 2007, **19**, 3559–3563.

72 M. A. Garcia, M. N. Ali, T. Parsons-Moss, P. D. Ashby and H. Nitsche, *Thin Solid Films*, 2008, **516**, 6261–6265.

73 M. A. Garcia, M. N. Ali, N. N. Chang, T. Parsons-Moss, P. D. Ashby, J. M. Gates, L. Stavsetra, K. E. Gregorich and H. Nitsche, *Nuclear Instruments and Methods in Physics Research, Section A: Accelerators, Spectrometers, Detectors and Associated Equipment*, 2008, **592**, 483–485.

74 M. N. Ali, M. A. Garcia, T. Parsons-Moss and H. Nitsche, *Nature Protocols*, 2010, **5**, 1440–1446.

75 E. S. Gillman, D. Costello, M. Moreno, A. Raspopin, R. Kasica and L. Chen, *Journal of Applied Physics*, 2010, **108**, year.

76 S. S. Kalagi, D. S. Dalavi, R. C. Pawar, N. L. Tarwal, S. S. Mali and P. S. Patil, *Journal of Alloys and Compounds*, 2010, **493**, 335–339.

77 S. J. Hong, H. Jun and J. S. Lee, *Scripta Materialia*, 2010, **63**, 757–760.

78 H. Ren, G. Xiang, G. Gu, X. Zhang, W. Wang, P. Zhang, B. Wang and X. Cao, *Journal of Nanomaterials*, 2012, **2012**, year.

79 F. Yue, W. Huang, Q. Shi, D. Li, Y. Hu, Y. Xiao, X. Deng and C. Wang, *Journal of Sol-Gel Science and Technology*, 2014, **72**, 565–570.

80 Q. Yi, P. Zhai, Y. Sun, Y. Lou, J. Zhao, B. Sun, B. Patterson, H. Luo, W. Zhang, L. Jiao, H. Wang and G. Zou, *ACS Applied Materials and Interfaces*, 2015, **7**, 18218–18224.

81 E. Breckenfeld, H. Kim, E. P. Gorzkowski, T. E. Sutto and A. PiquÃľ, *Applied Surface Science*, 2017, **397**, 152–158.

82 M. Jain, E. Bauer, Y. Lin, H. Wang, A. K. Burrell, T. M. McClesky and Q. X. Jia, *Integrated Ferroelectrics*, 2008, **100**, 132–139.

83 E. Bauer, A. H. Mueller, I. Usov, N. Suvorova, M. T. Janicke, G. I. N. Waterhouse, M. R. Waterland, Q. X. Jia, A. K. Burrell and T. M. McCleskey, *Advanced Materials*, 2008, **20**, 4704–4707.

84 S. M. Baber, Q. Lin, G. Zou, N. Haberkorn, S. A. Baily, H. Wang, Z. Bi, H. Yang, S. Deng, M. E. Hawley, L. Civale, E. Bauer, T. M. McCleskey, A. K. Burrell, Q. Jia and H. Luo, *The Journal of Physical Chemistry C*, 2011, **115**, 25338–25342.

85 R. Cobas, S. Muoz-Perez, J. M. Cadogan, T. Puig and X. Obradors, *Applied Physics Letters*, 2011, **99**, year.

86 J. M. Vila-FungueiriÃśo, B. Rivas-Murias and F. Rivadulla, *Thin Solid Films*, 2014, **553**, 81–84.

87 Y. H. Chuai, H. Z. Shen, Y. D. Li, B. Hu, Y. Zhang, C. T. Zheng and Y. D. Wang, *RSC Advances*, 2015, **5**, 49301–49307.

88 C. Xie, L. Shi, J. Zhao, Y. Li, S. Zhou and D. Yao, *Applied Surface Science*, 2015, **351**, 188–192.

89 Y. Lin, D. Y. Feng, M. Gao, Y. D. Ji, L. B. Jin, G. Yao, F. Y. Liao, Y. Zhang and C. L. Chen, *Journal of Materials Chemistry C*, 2015, **3**, 3438–3444.

90 C. Xie and L. Shi, *Applied Surface Science*, 2016, **384**, 459–465.

91 D. Yao, L. Shi, S. Zhou, H. Liu, J. Zhao, Y. Li and Y. Wang, *Journal of Applied Physics*, 2016, **119**, year.

92 H. Wang, B. Patterson, J. Yang, D. Huang, Y. Qin and H. Luo, *Applied Materials Today*, 2017, **9**, 402–406.

93 H. Luo, Y. Lin, H. Wang, C. Y. Chou, N. A. Suvorova, M. E. Hawley, A. H. Mueller, F. Ronning, E. Bauer, A. K. Burrell, M. McCieskey and Q. X. Jia, *Journal of Physical Chemistry C*, 2008, **112**, 20535–20538.

94 G. Zou, M. Jain, H. Zhou, H. Luo, S. A. Baily, L. Civale, E. Bauer, T. M. McCleskey, A. K. Burrell and Q. Jia, *Chemical Communications*, 2008, 6022–6024.

95 H. Luo, Y. Lin, H. Wang, J. H. Lee, N. A. Suvorova, A. H. Mueller, A. K. Burrell, T. M. McCleskey, E. Bauer, I. O. Usov, M. E. Hawley, T. G. Holesinger and Q. Jia, *Advanced Materials*, 2009, **21**, 193–197.

96 Y. Zhang, N. Haberkorn, F. Ronning, H. Wang, N. A. Mara, M. Zhuo, L. Chen, J. H. Lee, K. J. Blackmore, E. Bauer, A. K. Burrell, T. M. McCleskey, M. E. Hawley, R. K. Schulze, L. Civale, T. Tajima and Q. Jia, *Journal of the American Chemical Society*, 2011, **133**, 20735–20737.

97 H. Luo, G. Zou, H. Wang, J. H. Lee, Y. Lin, H. Peng, Q. Lin, S. Deng, E. Bauer, T. M. McCleskey, A. K. Burrell and Q. Jia, *Journal of Physical Chemistry C*, 2011, **115**, 17880–17883.

98 G. Zou, H. Wang, N. Mara, H. Luo, N. Li, Z. Di, E. Bauer, Y. Wang, T. McCleskey, A. Burrell, X. Zhang, M. Nastasi and Q. Jia, *Journal of the American Chemical Society*, 2010, **132**, 2516–2517.

99 G. Zou, H. Luo, Y. Zhang, J. Xiong, Q. Wei, M. Zhuo, J. Zhai, H. Wang, D. Williams, N. Li, E. Bauer, X. Zhang, T. M. McCleskey, Y. Li, A. K. Burrell and Q. X. Jia, *Chemical Communications*, 2010, **46**, 7837–7839.

100 R. E. Jilek, E. Bauer, A. K. Burrell, T. M. McCleskey, Q. Jia, B. L. Scott, M. F. Beaux, T. Durakiewicz, J. J. Joyce, K. D. Rector, J. Xiong, K. Gofryk, F. Ronning and R. L. Martin, *Chemistry of Materials*, 2013, **25**, 4373–4377.

101 G. Zou, H. Luo, F. Ronning, B. Sun, T. M. McCleskey, A. K. Burrell, E. Bauer and Q. X. Jia, *Angewandte Chemie - International Edition*, 2010, **49**, 1782–1785.

102 S. A. Chambers, *Surface Science Reports*, 2000, **39**, 105–180.

103 D. G. Schlom, L. Q. Chen, X. Pan, A. Schmehl and M. A. Zurbuchen, *Journal of the American Ceramic Society*, 2008, **91**, 2429–2454.

104 J. Cao and J. Wu, *Materials Science and Engineering R: Reports*, 2011, **71**, 35–52.

105 P. Schiffer, A. P. Ramirez, W. Bao and S.-W. Cheong, *Phys. Rev. Lett.*, 1995, **75**, 3336–3339.

106 J. M. Vila-FungueiriÃśo, B. Cong Tinh, B. Rivas-Murias, E. Winkler, J. Milano, J. Santiso and F. Rivadulla, *Journal of Physics D: Applied Physics*, 2016, **49**, 315001.

107 M. Jain, P. Shukla, Y. Li, M. Hundley, H. Wang, S. Foltyn, A. Burrell, T. McCleskey and Q. Jia, *Advanced Materials*, 2006, **18**, 2695–2698.

108 I. Lucas, J. M. Vila-FungueiriÃśo, P. JimÃľnez-Cavero, B. Rivas-Murias, C. MagÃľn, L. MorellÃşn and F. Rivadulla, *ACS Applied Materials & Interfaces*, 2014, **6**, 21279–21285.

109 J. M. Vila-FungueiriÃśo, B. Rivas-Murias, B. RodrÃ■guez-GonzÃąlez and F. Rivadulla, *Chemistry of Materials*, 2014, **26**, 1480–1484.

110 L. Balcells, L. Abad, H. Rojas, A. P. d. Pino, S. Estrade, J. Arbiol, F. Peiro and B. Martinez, *Journal of Applied Physics*, 2008, **103**, 07E303.

111 L. Iglesias, A. Sarantopoulos, C. Magén and F. Rivadulla, *Phys. Rev. B*, 2017, **95**, 165138.

112 L. B. Wang, A. Maignan, D. Pelloquin, S. HÃľbert and B. Raveau, *Journal of Applied Physics*, 2002, **92**, 124–128.

113 A. Maignan, S. HÃľbert, M. Hervieu, C. Michel, D. Pelloquin and D. Khomskii, *Journal of Physics Condensed Matter*, 2003, **15**, 2711–2723.

114 T. Sun, J. Ma, Q. Y. Yan, Y. Z. Huang, J. L. Wang and H. H. Hng, *Journal of Crystal Growth*, 2009, **311**, 4123–4128.

115 B. Rivas-Murias, J. M. Vila-FungueiriÃśo and F. Rivadulla, *Scientific Reports*, 2012, **5**, 11889.

116 I. Lucas, P. Jiménez-Cavero, J. M. Vila-Fungueiriño, C. Magén, S. Sangiao, J. M. de Teresa, L. Morellón and F. Rivadulla, *Phys. Rev. Materials*, 2017, **1**, 074407.

117 H. Luo, H. Yang, S. A. Baily, O. Ugurlu, M. Jain, M. E. Hawley, T. M. McCleskey, A. K. Burrell, E. Bauer, L. Civale, T. G. Holesinger and Q. Jia, *Journal of the American Chemical Society*, 2007, **129**, 14132–14133.

118 L. H. Yan, W. Z. Liang, S. H. Liu, W. Huang and Y. Lin, *Integrated Ferroelectrics*, 2011, **131**, 82–88.

119 M. Zhou, Y. Li, I. Jeon, Q. Yi, X. Zhu, X. Tang, H. Wang, L. Fei, Y. Sun, S. Deng, Y. Matsuo, H. Luo and G. Zou, *Sci Rep*, 2016, **6**, 26390.

120 R. Dargis, A. Clark, F. E. Arkun, T. Grinys, R. Tomasiunas, A. O'Hara and A. A. Demkov, *Journal of Vacuum Science & Technology A: Vacuum, Surfaces, and Films*, 2014, **32**, 041506.

121 K. J. Hubbard and D. G. Schlom, *Journal of Materials Research*, 1996, **11**, 2757âĂŞ2776.

122 S. R. Bakaul, C. R. Serrao, M. Lee, C. W. Yeung, A. Sarker, S.-L. Hsu, A. K. Yadav, L. Dedon, L. You, A. I. Khan, J. D. Clarkson, C. Hu, R. Ramesh and S. Salahuddin, *Nature Communications*, 2016, **7**, 10547.

123 J. M. Vila-FungueiriÃśo, R. Bachelet, G. Saint-Girons, M. Gendry, M. Gich, J. Gazquez, E. Ferain, F. Rivadulla, J. Rodriguez-Carvajal, N. Mestres and A. Carretero-Genevrier, *Frontiers in Physics*, 2015, **3**, 38.

124 A. GÃşmez, J. M. Vila-FungueiriÃśo, R. Moalla, G. Saint-Girons, J. GÃązquez, M. Varela, R. Bachelet, M. Gich, F. Rivadulla and A. Carretero-Genevrier, *Small*, 2017, **13**, n/a–n/a.

125 Z. Jovanovic, M. Spreitzer, U. Gabor and D. Suvorov, *RSC Advances*, 2016, **6**, 82150–82156.

126 P. Gupta and J. Narayan, *Journal of Applied Physics*, 2014, **115**, 043513.

127 A. Carretero-Genevrier, R. Bachelet, G. Saint-Girons, R. Moalla, J. M. Vila-FungueiriÃśo, B. Rivas-Murias, F. Rivadulla, J. Rodriguez-Carvajal, A. Gomez, J. Gazquez, M. Gich, N. Mestres, A. Tiwari, R. A. Gerhardt and M. Szutkowska, in *Development of Epitaxial Oxide Ceramics Nanomaterials Based on Chemical Strategies on Semiconductor Platforms*, John Wiley Sons, Inc., 2016, pp. 1–32.

128 W. Sun, J.-Y. Liu, X.-Q. Gong, W.-Q. Zaman, L.-M. Cao and J. Yang, *Scientific Reports*, 2016, **6**, 38429.

129 G. C. da Silva, M. R. Fernandes and E. A. Ticianelli, *ACS Catalysis*, 2018, **8**, 2081–2092.

130 E. Breckenfeld, H. Kim, E. P. Gorzkowski, T. E. Sutto and A. PiquÃľ, *Applied Surface Science*, 2017, **397**, 152 – 158.